Calcium flares and compartmentalization in rod photoreceptors

Yunzhen Li[a,1], Fabio Falleroni[a,1], Simone Mortal[a,1], Ulisse Bocchero[a,1,2], Dan Cojoc[b], and Vincent Torre[a,c,3]

[a]Neurobiology Department, International School for Advanced Studies (SISSA), Trieste 34136, Italy; [b]Institute of Materials, National Research Council of Italy (CNR), 34149 Trieste, Italy; and [c]Joint Laboratory of Biophysics and Translational Medicine, Institute of Systems Medicine (ISM)–SISSA, 215123 Suzhou, Jiangsu, P. R. China

Edited by Gordon L. Fain, University of California, Los Angeles, CA, and accepted by Editorial Board Member Jeremy Nathans July 20, 2020 (received for review March 14, 2020)

Rod photoreceptors are composed of a soma and an inner segment (IS) connected to an outer segment (OS) by a thin cilium. OSs are composed of a stack of ∼800 lipid discs surrounded by the plasma membrane where phototransduction takes place. Intracellular calcium plays a major role in phototransduction and is more concentrated in the discs, where it can be incorporated and released. To study calcium dynamics in rods, we used the fluorescent calcium dye CaSiR-1 AM working in the near-infrared (NIR) (excitation at 650 and emission at 664 nm), an advantage over previously used dyes. In this way, we investigated calcium dynamics with an unprecedented accuracy and most importantly in semidark-adapted conditions. We observed light-induced drops in $[Ca^{2+}]_i$ with kinetics similar to that of photoresponses recorded electrophysiologically. We show three properties of the rods. First, intracellular calcium and key proteins have concentrations that vary from the OS base to tip. At the OS base, $[Ca^{2+}]_i$ is ∼80 nM and increases up to ∼200 nM at the OS tip. Second, there are spontaneous calcium flares in healthy and functional rod OSs; these flares are highly localized and are more pronounced at the OS tip. Third, a bright flash of light at 488 nm induces a drop in $[Ca^{2+}]_i$ at the OS base but often a flare at the OS tip. Therefore, rod OSs are not homogenous structures but have a structural and functional gradient, which is a fundamental aspect of transduction in vertebrate photoreceptors.

photoreceptors | calcium | phototransduction

Rod outer segments (OSs) are composed of a stack of ∼800 lipid discs surrounded by the plasma membrane where the phototransduction machinery is located (1, 2). The OS is connected to the soma through a narrow structure called the cilium (3), providing an electrical connection so that electrical signals generated in the OS are transmitted to the soma. The soma is composed of an inner segment (IS) containing the nucleus and from which the synaptic terminals protrude. The OS is not a well-mixed compartment and appears to be rather inhomogeneous: The composition of the disk membrane varies from the base of the OS (where new discs are synthesized) to its tip (where old discs are continuously shed) (4–8).

The complex dynamics of disk renewal and the changes in disk composition along the OS suggest a variable efficiency of phototransduction. Indeed, some classic (9, 10) and more recent (11) works have shown that the amplitude of the single photoresponse and of the maximal photoresponse is higher at the base and two to three times smaller at the OS tip (12). The unequal sensitivity along the OS could be related to the availability of metabolic energy in the form of NADPH. Indeed, Miyagishima et al. have shown that the recovery of sensitivity after light stimuli is slower at the OS tip than at its base (13). Furthermore, localized light-induced changes in cGMP and Ca^{2+} concentrations decay along the OS from the point of stimulation, suggesting a mechanism that limits the spread of adaptation to light (14).

In this context, Ca^{2+} plays a fundamental role in regulating light adaptation (15, 16), recovery after pigment bleaching (17, 18), and OS structural stability (19, 20). To study calcium along the OS, we used CaSiR-1 AM (excitation 650 nm, emission 664 nm) (21) and Fura Red (excitation 440 and 480 nm, emission ∼650 nm); we analyzed its intracellular dynamics in dissociated rod photoreceptors composed of an IS and an OS (IS+OS) and in small pieces of retina obtained from *Xenopus laevis* frogs. CaSiR-1 increases fluorescence emission upon binding calcium, while Fura Red decreases its emission following binding to calcium. The excitation with Fura Red at two wavelengths allows a quantitative estimation of intracellular calcium by what is referred to as ratiometric calcium imaging (22). Conversely, CaSiR-1 AM allows the study of calcium dynamics in rods under semidark-adapted conditions.

This dye has only recently been used to investigate Ca^{2+} in rod photoreceptors (23). In rods loaded with CaSiR-1, we directly observed a light-induced drop in fluorescence, with kinetics very similar to that of photoresponses recorded electrophysiologically. Therefore, it is possible to follow calcium dynamics using an excitation light at 650 nm, which reduces the amplitude of a saturating photoresponse induced by a flash of light at 488 nm of approximately ∼30–40%. The use of CaSiR-1 allowed us to study Ca^{2+} in rods with unprecedented accuracy and resolution and in semidark-adapted conditions.

Our experiments highlight several properties of rods: First, OSs have a strong gradient not only in responsiveness but also in $[Ca^{2+}]_i$, which is higher at the tip than at the OS base; second, in

Significance

Rod photoreceptor outer segments (OSs) are specialized ciliary architectures. Our imaging experiments reveal three properties of rods. First, intracellular calcium and key proteins have a concentration varying from the OS base to the tip. At the OS base, $[Ca2+]_i$ is approximately 80 nM and increases up to ∼200 nM at the OS tip; second, there are spontaneous calcium flares in functional OSs, and these flares are highly localized and are more pronounced at the OS tip; third, a bright flash of light at 488 nm induces a drop in $[Ca2+]_i$ at the OS base but often a flare at the OS tip. This structural and functional gradient of the phototransduction machinery is a fundamental aspect of transduction in vertebrate photoreceptors.

Author contributions: U.B. and V.T. conceived and discussed the idea; F.F., S.M., U.B., and V.T. designed research; Y.L., F.F., S.M., and U.B. performed research; Y.L., F.F., S.M., and U.B. analyzed data; and S.M., U.B., D.C., and V.T. wrote the paper.

The authors declare no competing interest.

This article is a PNAS Direct Submission. G.L.F. is a guest editor invited by the Editorial Board.

[1]Y.L., F.F., S.M., and U.B. contributed equally to this work.

[2]Present address: Photoreceptor Physiology Group, National Eye Institute (NEI), NIH, Bethesda, MD 20892.

[3]To whom correspondence may be addressed. Email: torre@sissa.it.

This article contains supporting information online at https://www.pnas.org/lookup/suppl/doi:10.1073/pnas.2004909117/-/DCSupplemental.

First published August 19, 2020.

semidark-adapted conditions, it is possible to observe spontaneous calcium flares, i.e., highly localized increases in $[Ca^{2+}]_i$ in healthy and functional rods; third, at the OS tip, a bright flash of light often induces a calcium flare and not a drop in $[Ca^{2+}]_i$.

Results

Strong Calcium Gradient in the Rod OS. When a dark-adapted retinal rod of a small piece of retina loaded with CaSiR-1 was briefly illuminated with 650-nm light, the rod ISs appeared rather bright *SI Appendix*, Fig. S1*A*). However, the OSs displayed a gradient of fluorescence that increased in intensity from the base to the tip of the rod (*SI Appendix*, Fig. S1*A*). When the CaSiR-1–loaded retinas were mechanically dissociated, the observation dish was full of isolated OS, which were uniformly bright (*SI Appendix*, Fig. S1*B*). The OSs that were still attached to the IS (IS+OS) displayed the same gradient of fluorescence observed in intact rods, which was more intense at the tip and decreased toward the base (Fig. 1*A*). The profile of fluorescence was similar in IS+OS rods across preparations, but the level of fluorescence at the base varied (Fig. 1*B*). IS+OS rods showing a clear gradient in CaSiR-1 fluorescence were usually functional: Illuminating these rods with a brief flash of light at 488 nm, we were able to measure a transient decrease of the emitted fluorescence on the order of 0.02–0.05 *DF/F* ((fluorescence at time t − fluorescence at time 0)/fluorescence at time 0), which was an indication of a light-induced drop in intracellular calcium (Fig. 1*C*). The time course of the change in *DF/F* was reminiscent of that observed in electrical recordings of photoresponses (23) (*SI Appendix*, Fig. S2*A*).

The steady light at 650 nm used to excite CaSiR-1 was approximately equivalent to 480 $R^*{\cdot}rod^{-1}{\cdot}s^{-1}$ and reduced the circulating dark current by ∼30–40% (*SI Appendix*, Fig. S2*B*), indicating that CaSiR-1 allowed resolution of calcium dynamics in semidark-adapted conditions. The ratio between functional IS+OS rods and the total rods present in the preparations, shown in Fig. 1*D*, indicates that our samples were relatively homogeneous across the experiments. Isolated OS or IS+OS rods not showing the brightness gradient along the OS (Fig. 1 *E* and *F*) did not show any light response and were considered nonfunctional (Fig. 1*H*). To check whether the brightness gradient seen in the OS of IS+OS rods was caused by a different loading, we repeated the same experiment by loading retinas with Fura Red. In this case, the fluorescence was brighter at the base and decreased toward the tip (Fig. 1*G*). Experiments of ratiometric calcium imaging using Fura Red indicate that in light-adapted conditions, $[Ca^{2+}]_i$ is approximately ∼80 nM at the base and ∼200 nM at the tip (*SI Appendix*, Fig. S3) and that its mean value is in the range of what has been previously reported (24). These results show that $[Ca^{2+}]_i$ is not homogeneous inside the rod OS and has a strong gradient.

Strong Gradient of Light Responsiveness. We stimulated isolated IS+OS rods with diffuse light at 488 nm (Fig. 2*A*) and measured CaSiR-1 fluorescence emitted at the base (Fig. 2 *B* and *E* dark red), the center (Fig. 2*B*, orange), and at the tip (Fig. 2*B*, green). We observed a clear light-induced decrease in *DF/F* in each rod compartment, but the drop in *DF/F* was larger at the base than at the tip ($(DF/F)_{base} - (DF/F)_{tip}$, or gradient in responsiveness for simplicity) (Fig. 1*C*) ($n = 15$; $P < 0.001$). This gradient in responsiveness along the OS is in agreement with the drop in sensitivity observed with electrical recordings with localized spots of light, along the OS (11). Interestingly, the drop in responsiveness was larger in intact rods from pieces of retina (hereafter referred to as "intact retinal rods") (Fig. 2 *D–F*), suggesting an important role for the integrity of the retinal tissue. In some of these rods, following a flash at 488 nm, no visible decrease in

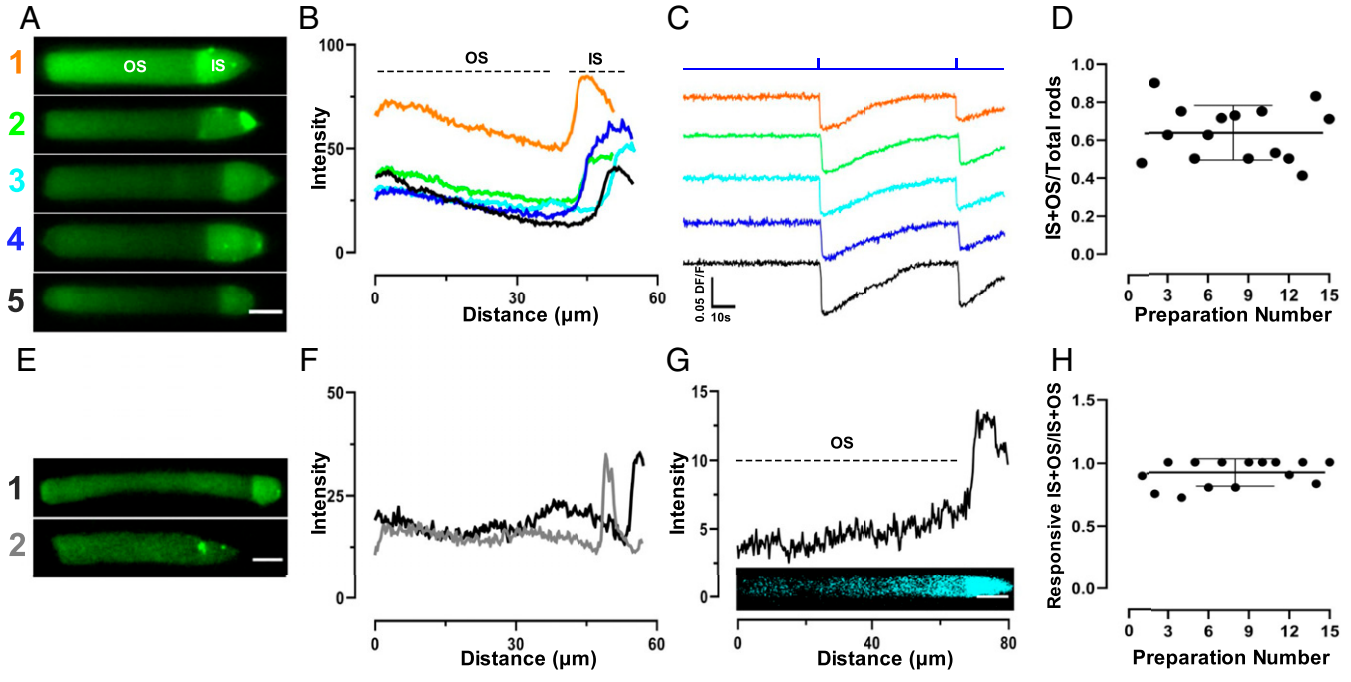

Fig. 1. Light-evoked calcium drops in IS+OS rods. (*A*) Fluorescence images of isolated IS+OS rods loaded with CaSiR-1. The IS is usually brighter than the OS. (*B*) Fluorescence intensity profile for the five IS+OS rods shown in *A*. (*C*) Light-evoked fluorescence drops evoked by a flash of light of 1 s, eliciting ∼2,100 R* per rod at 488 nm at the times indicated by the blue trace at the top of the image. The slight decrease of *DF/F* observed at the second flash of light is caused by dye bleaching. In *A–C*, the same color corresponds to the same rod. (*D*) Ratio of the number of isolated IS+OS over the total number of rods present in the preparations ($n = 15$ experiments, 0.6368 ± 0.145). (*E*) Example of two unresponsive rods. (*F*) As in *B* but for two IS+OS shown in *E*. (*G*) Fluorescence intensity profile for an IS+OS rod loaded with Fura Red in light-adapted conditions. *Top* is the intensity profile, and at *Bottom* is the fluorescence image. In this case, the base of the OS is brighter than the tip. (Scale bars, 10 μm.) (*H*) Responsiveness ratio between IS+OS rods ($n = 15$ experiments, 0.92 ± 0.108).

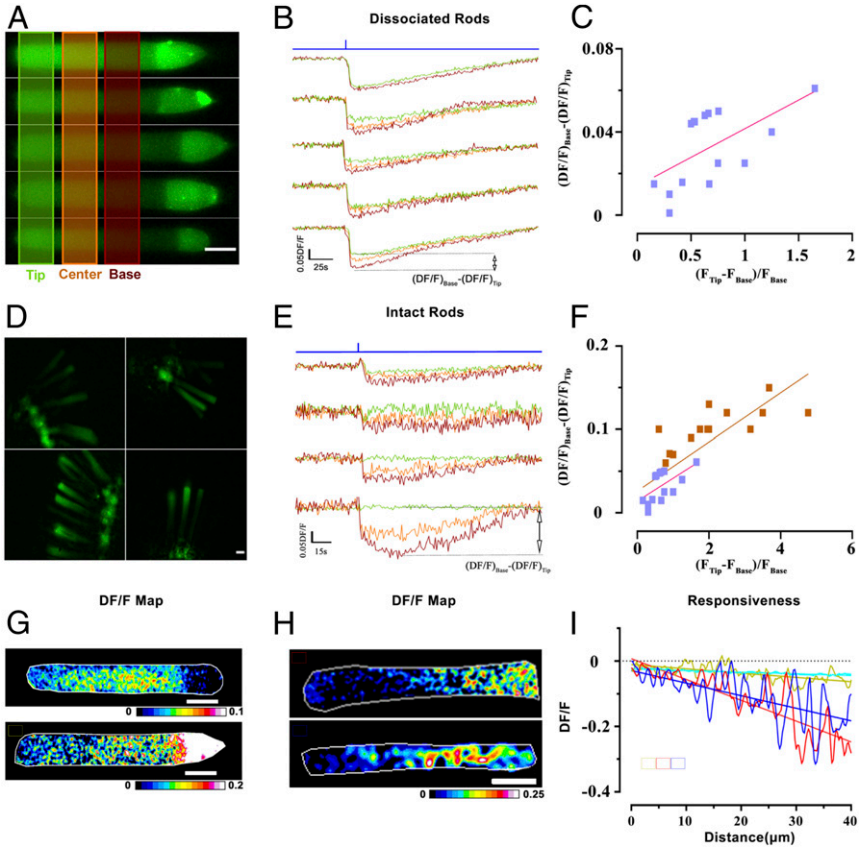

Fig. 2. Gradient of light-evoked calcium drops. (*A*) Rods fluorescence images of Fig. 1*A*. The green (tip), orange (center), and dark red (base) semitransparent stripes indicate the regions of the OS. (*B*) Light-evoked *DF/F* drops, for five rods in *A*, at the tip, center, and base (traces colors as stripes in *A*). The evoked *DF/F* of the three regions are superimposed. Light stimulus of 1 s, eliciting ~2,100 R* per rod. (*C*) Relation between calcium gradient ($DF/F_{base} - DF/F_{tip}$) and response gradient ($(F_{tip} - F_{base})/F_{base}$) for $n = 15$ rods. The straight red line is a linear fit given by $y = 0.02075 \times x + 0.03047$ (R^2: 0.3431). Fluorescent images pieces of retina loaded with CaSiR-1 (*D*): DF/F for intact retinal rods ($n = 4$) at the base, center, and tip with diffuse illumination and the same color coding as in *B* (*E*). (*F*) Fit for intact retinal rods ($n = 15$, brown points) superimposed over the graph in *C*; the straight brown line is a linear fit given by $Y = 0.02945*X + 0.02607$ (R^2: 0.6707). (*G*) Gradients of responsiveness of two dissociated rods (scale bar *DF/F*). (*H*) Gradients of responsiveness of two rods from pieces of retinas. (*I*) Dependence of responsiveness (*DF/F*) along the OS length for *G* and *H*. (Scale bars, 10 μm.).

fluorescence was detected at the tip of the OS (Fig. 2*E*, green trace). However, a clear decrease in fluorescence was observed at the base of the OS (Fig. 2*E*, dark red trace) ($n = 15$; $P < 0.001$).

Collected data from 15 IS+OS rods and 15 intact retinal rods showed that the drop in responsiveness was correlated to the relative amplitude of increase of the fluorescence emitted by CaSiR-1 ($(F_{tip} - F_{base})/F_{base}$) at the OS tip (Fig. 2 *C* and *F*), mirroring the increase of $[Ca^{2+}]_i$ measured with Fura Red (Fig. 1*G* and *SI Appendix*, Fig. S3). A better visualization of the gradient in responsiveness is obtained by the map of *DF/F*, where *F* is the fluorescence in a time window of 1 s before the light flash at 488 nm and *DF* is the fluorescence drop caused by the light in a time window of 1 s centered around the time of maximum fluorescence drop. This map was obtained in dissociated rods (Fig. 2*G*) and in rods from pieces of retinas (Fig. 2*H*), showing a clear gradient in responsiveness falling at the center of the OS. From these maps, we obtained the profile of responsiveness along the OS by averaging the values of *DF/F* along the direction perpendicular to the OS (Fig. 2*I*).

To analyze in greater detail the time course of the light-induced calcium changes, we averaged the light-induced drop in fluorescence over the first five photoresponses. The emitted fluorescence and possibly $[Ca^{2+}]_i$ fell with a fast and a slower component (*SI Appendix*, Fig. S2 *A–C*), as predicted from the model of ref. 16. The fast drop in calcium was caused by the closure of light-sensitive channels permeable to Ca^{2+} ions, and the slower component was associated with the dynamics of intracellular (native and exogenous, such as the introduced dye) Ca^{2+} buffers.

The experiments illustrated in Figs. 1 and 2 were obtained with diffuse illumination at 488 nm. To explore the response to highly localized flashes of light, we used a confocal microscope allowing illumination with blue light at 488 nm of specific regions of the OS (see colored boxes in Fig. 3 *A* and *B*, *Left*). When we illuminated a region of ~5 × 5 μm^2 at the base (Fig. 3*A*), we observed a clear light-induced calcium decrease, whereas no response at the center or at the tip of the OS was detected. We also illuminated the bright IS with the same light, and we could not detect any light-induced fluorescence decrease (Fig. 3*B*). We constructed a map of responsiveness along the OS when the same spot of illuminating light was moved along its axis. Data collected from six experiments showed that with confined illumination, there was a marked decrease in responsiveness from the base to the tip of the OS (Fig. 3*C*) ($n = 6$; $P < 0.001$). The trend of responsiveness obtained with localized illumination was similar to that obtained with diffuse illumination, but in this case the change in fluorescence was measured in localized regions.

Spontaneous Calcium Flares. During imaging recordings (~8–15 min) of the fluorescence emitted by CaSiR-1, we observed spontaneous calcium flares i.e., spontaneous bursts of increased

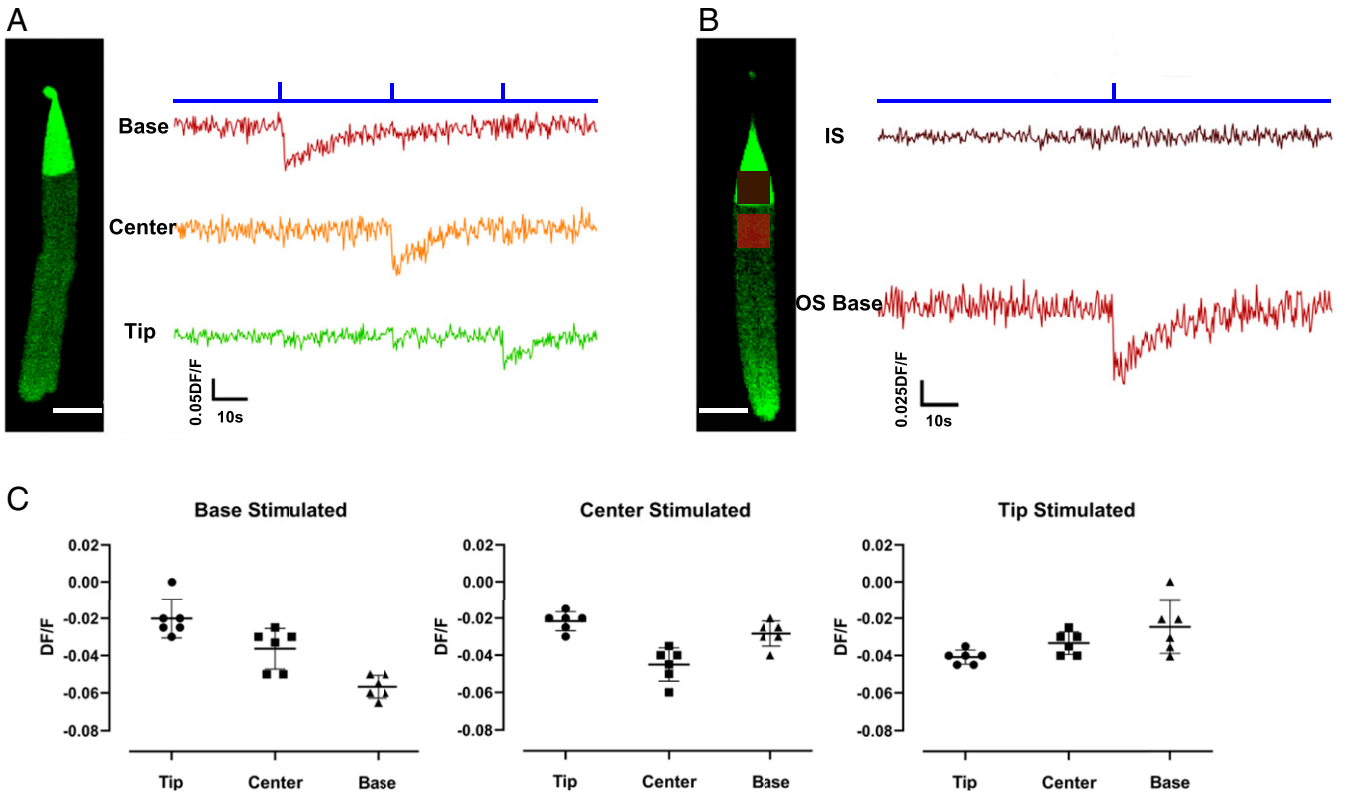

Fig. 3. Calcium drops in response to localized illuminations. (*A*) The fluorescence image shows an example of an IS+OS rod loaded with CaSiR-1 and the colored boxes indicate where the localized illumination of 1 s at the base (dark red), center (orange), and tip (green), eliciting ~1,500 R* per rod was applied. Colored traces were obtained from averaging fluorescence changes inside the boxes on the *Left* with the same color. The blue line indicates the timing of the localized illumination. (*B*) As in *A* but for a localized illumination of the IS (brown) and the OS base (dark red). (*C*) Quantification of the *DF/F* changes in response to localized stimuli ($n = 6$; base stimulation *DF/F*: $\text{mean}_{\text{base}}$ −0.057 ± 0.002 SEM, $\text{mean}_{\text{center}}$ −0.036 ± 0.004 SEM, mean_{tip} −0.020 ± 0.004 SEM; center stimulation *DF/F*: $\text{mean}_{\text{base}}$ −0.028 ± 0.003 SEM, $\text{mean}_{\text{center}}$ −0.045 ± 0.004 SEM, mean_{tip} −0.022 ± 0.002 SEM; tip stimulation *DF/F*: $\text{mean}_{\text{base}}$ −0.024 ± 0.006 SEM, $\text{mean}_{\text{center}}$ −0.033 ± 0.002 SEM, mean_{tip} −0.041 ± 0.002 SEM; Student's *t* test mean_{tip} (tip stimulation) vs. $\text{mean}_{\text{base}}$ (base stimulation) $P < 0.001$). (Scale bars, 10 μm.)

fluorescence, both in isolated rods (Fig. 4 *A* and *B*) and in intact retinal rods (Fig. 4*C*). These flares (see red stars in Fig. 4*A*) occurred more often at the tip than at the center or base of the rods, and only occasionally spontaneous flares were seen at the base of the rods. The rods that exhibited calcium flares were functional, and a bright flash at 488 nm induced the expected drop in intracellular calcium (Fig. 4*A*). Calcium flares in isolated rods (Fig. 4*B*) and in intact retinal rods (Fig. 4*C*) had a similar amplitude, occurred preferentially at the tip, and occasionally could also be seen in the IS (see bottom traces in Fig. 4 *B* and *C*).

Calcium flares could be triggered by light flashes at 488 nm. In the experiment illustrated in Fig. 4 *D* and *E*, diffuse light flashes induced the usual drop in intracellular calcium at the base of the OS (dark red trace), but at the center of the OS, we measured a large increase in *DF/F* of ~0.45 (orange trace in Fig. 4*E*) (*SI Appendix*, Fig. S4). The occurrence of these flares was not associated with the death of the rod, as after the appearance of one flare, it was still possible to observe a light-induced calcium decrease (Fig. 4 *D* and *E*). The calcium flare occurring in the middle of the OS remained localized and did not propagate to the neighboring portion of the OS. Similarly, flares occurring in the IS did not propagate in any appreciable way into the OS. In several of these experiments, we collected not only fluorescence images (Fig. 4 *F*, *Left*) but also bright field images (Fig. 4 *F*, *Right*) of the rod, verifying the physical integrity of the rod during and after a calcium flare. We mapped the localization of both flares, spontaneous as well as induced by a 488-nm flash light along the OS and collected data from 30 experiments, showing that these flares occurred primarily at the tip of the OS (Fig. 4*G*). Flares were similar in dissociated (Fig. 4*H*) and intact rods (Fig. 4*I*) (*SI Appendix*, Fig. S5). Therefore, transient and spontaneous bursts of $[Ca^{2+}]_i$ occurring in the OS, primarily at its center and tip, occurred in healthy rods with similar properties in dissociated and intact retinal rods. It is possible, however, that these $[Ca^{2+}]_i$ flares occur at locations inside the OS where the phototransduction pathways physiologically lose their efficiency.

Coupling of Calcium in the OS and IS. The OS and IS are connected by the cilium, which allows the transmission of electrical signals generated in the OS to the IS (25). The cilium also allows the migration of large proteins synthesized in the nucleus necessary for the maintenance of the biological integrity of the OS (26). Therefore, it is of interest to see how changes in intracellular calcium occurring in the OS or IS propagate through the cilium. We recently showed that a single stimulation or a train of three mechanical stimulations of ~15 pN locally applied either to the IS or OS induce a transient and localized increase in $[Ca^{2+}]_i$ (23). Therefore, it is possible to induce localized transient increases in $[Ca^{2+}]_i$ by mechanical stimulations and by light flashes, allowing the propagation of $[Ca^{2+}]_i$ transients through the cilium to be investigated. As shown in Fig. 5, localized increases in $[Ca^{2+}]_i$ caused by the mechanical stimulation of either the OS (Fig. 5*A*) or the IS (Fig. 5*B*) do not propagate across the cilium. Similarly, a green light at 488 nm induces a drop in $[Ca^{2+}]_i$ at the base of the OS, which does not propagate to the IS

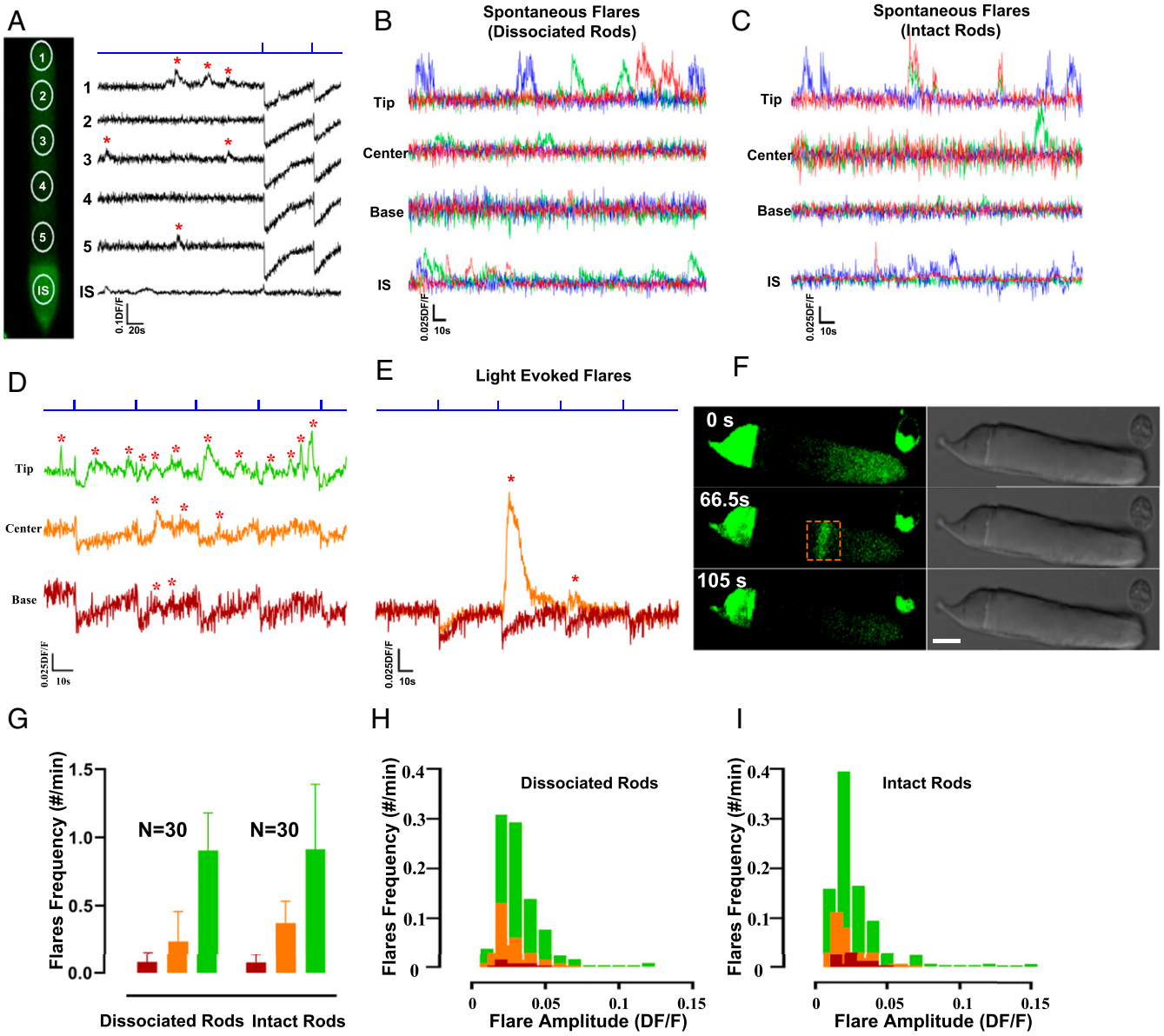

Fig. 4. Calcium flares. (*A*) IS+OS loaded with CaSiR-1. DF/F from five regions circled, showing spontaneous flares (red stars). Immediately after, two light-evoked *DF/F* drops. Light flashes of 1 s, eliciting ~2100 R* per rod; timing indicated by blue trace. (*B* and *C*) Magnification of the *DF/F* changes induced by spontaneous flares in isolated rods (*B*) and in rods from pieces of retina (*C*). Different colors represent different rods. (*D*) Spontaneous flares and light-evoked drops of *DF/F* at the tip, center, and base of an intact rod. (*E*) Light-evoked calcium flares. Light flashes in *A*. (*F*) Fluorescence and DIC images before, during, and after the calcium flare shown in *E*. The calcium flare (red box) remained localized and the rod remained unaltered. (Scale bar, 10 μm.) (*G*) Occurrence of calcium flares in isolated rods and pieces of retinas. Dissociated IS+OS $n = 30$, flare frequency: $\text{mean}_{\text{base}}$ 0.081 ± 0.03 SEM, $\text{mean}_{\text{center}}$ 0.238 ± 0.089 SEM, mean_{tip} 0.905 ± 0.112 SEM, $P < 0.001$ tip vs. base; intact retinal rods $n = 30$, flare frequency: $\text{mean}_{\text{base}}$ 0.077 ± 0.024 SEM, $\text{mean}_{\text{center}}$ 0.372 ± 0.066 SEM, mean_{tip} 0.914 ± 0.194 SEM, $P < 0.001$ tip vs. base. (*H* and *I*) Frequency of spontaneous calcium flares with an amplitude equal to DF/F at tip (green), center (orange), and base (dark red) in dissociated IS+OS ($n = 30$) and pieces of retinas ($n = 30$).

(Fig. 5*C*). Therefore, the cilium acts as a powerful blocker of calcium propagation flow between the OS and IS. The blockage of calcium propagation across the cilium could be caused by buffering organelles around it (27). Therefore, we tested the buffering ability of mitochondria by using the MitoTracker mitochondrial label. We found clusters of mitochondria in the IS close to the cilium (a comparison of the bright field images with the Red staining of mitochondria is shown in Fig. 5*D*). A similar observation has already been made in cones where mitochondria form a dense cluster that acts as a diffusion barrier between the OS and the IS (28). These mitochondria were mobile and moved by 1–3 microns per minute, remaining localized in the IS. However, a bright flash of light at 488 nm (see the blue arrow in Fig. 5*E*) drove the mitochondrial motion in a direction opposite to the location of the cilium and the OS (Fig. 5 *E*, *F*, *J*, and *K*) (*SI Appendix*, Fig. S6). These results suggest that mitochondria in the rod IS could be the molecular structures impeding the flow of intracellular calcium between the OS and IS and that their location could be modified by light.

Structural and Functional Gradient in the OS. To confirm and analyze the presence of the structural gradient along the OS, we examined the longitudinal profile of some components of the cytoskeleton and of the cell membranes. We found that the concentration of actin (Fig. 6 *A*, *D*, and *G*); tubulin (Fig. 6 *B*, *E*, and *H*), and cholesterol (Fig. 6 *C*, *F*, and *I*) along the OS is not

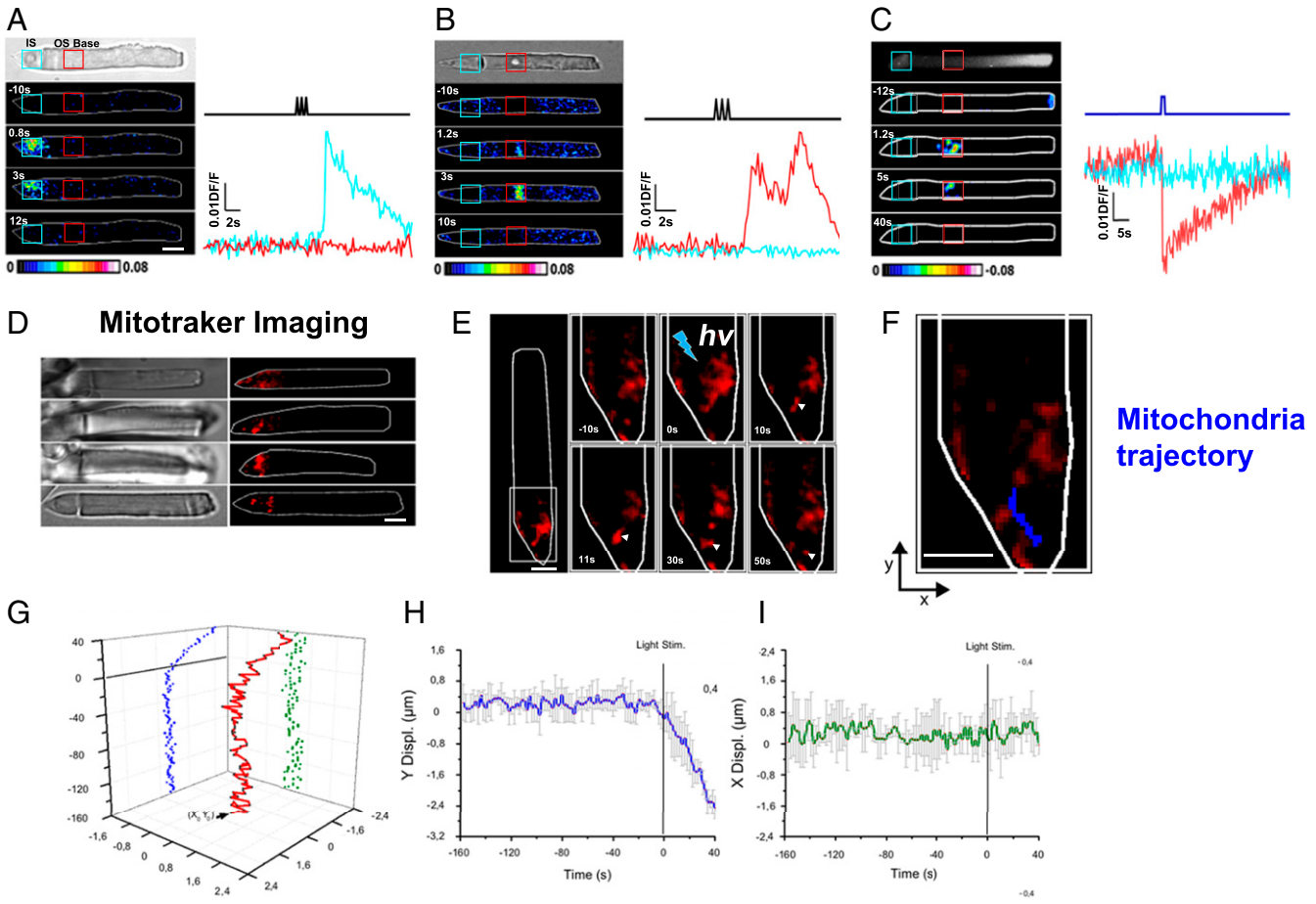

Fig. 5. Compartmentalization of calcium dynamics between IS and OS. (*A*) *DF/F* transients evoked by a mechanical stimulation of the IS. The force was ~8 pN for each mechanical pulse. Bright-field image at *Top*. Below, *DF/F* maps before, during, and after the stimulus, with respective timing. (*B*) As in *A*, but for the OS. (*C*) Localized light stimulation of the OS base with a 488-nm light pulse of 1 s, equivalent to ~2,100 R* per rod. (*D*) Map of MitoTracker labeling indicating the localization of mitochondria in four rods: bright-field images (*Left*) and the fluorescence emitted by Mitotracker (*Right*). (*E*) Images of mitochondria over ~1 min and the effect of a bright flash of diffuse light at 488 nm. (*F*) In blue, the trajectory of mitochondria following a light stimulation of 1 s and ~2100 R* per rod. (*G*) Three-dimensional plot of mitochondria trajectory (*x*, *y*, Time), horizontal bar indicates the light stimulus. (*H*) Average mitochondria displacement on the *y* axes. The vertical bar represents the light stimulus onset (blue trace is the mean, and the bars represent the SEM) ($n = 5$). (*I*) As in *H*, but for the *x* axes ($n = 5$). (Scale bars, 10 μm.)

homogeneous and that immunolabeling of these molecules is more evident at the OS base and less evident at the OS tip. Therefore, OS is not only functionally inhomogeneous but also structurally inhomogeneous, and some hints of structural non-uniformity are present in the distribution profiles of proteins and lipids obtained by combining serial sectioning of the retina with quantitative mass spectrometry (29). The spatial resolution of these profiles, however, is not adequate to establish in a conclusive way the existence of gradients of structural proteins inside the OS, and similar data with better spatial resolution are needed.

Discussion

Our work reveals and confirms that several functional (Figs. 1–5) and structural properties (Fig. 6) of the rod OS vary longitudinally: there is a sharp gradient of $[Ca^{2+}]_i$, responsiveness, the occurrence of calcium flares, and the structural components of OS (summarized in Fig. 7). Early (29) and more recent electron micrographs (30) of the rod OS show a perfect stack of discs in the OS, which have the same shape and geometrical dimensions from the base to its tip. In contrast with these pictures, however, the rod OS is not a homogeneous structure and displays both a functional and a structural gradient, where new discs are synthetized and shed (31). The present manuscript also describes a—to some extent—unexpected feature of the rod OS: the existence of spontaneous and light-induced calcium flares, i.e., highly localized increases in $[Ca^{2+}]_i$.

Calcium Flares. The observation of 488-nm light-induced flares of $[Ca^{2+}]_i$ (see Fig. 4 and see *SI Appendix*, Figs. S4 and S5) at the center and tip of the rod OSs, both in isolated rods and in intact retinal rods, is remarkable and unexpected. However, it has been previously shown that upon light stimulation, calcium can be released from the discs (19, 20). This evidence suggests that light stimuli can transiently and locally increase $[Ca^{2+}]_i$ in the OS. The calcium flares described here were observed using the fluorescent dye CaSiR-1, which works when excited at 650 nm and, therefore, not under conditions of dark adaptation. Indeed, calcium flares can also appear during imaging recordings of the fluorescence emitted by CaSiR-1, and their occurrence is random (Fig. 4 *B* and *C*). It is possible, therefore, that the observed calcium flares occur as a consequence of the activation of rhodopsin on the discs: Indeed, on some occasions, we observed that following several minutes of continuous stimulation at 650 nm, light flashes at 488 nm induced calcium flares more frequently, as shown in the recording of *SI Appendix*, Fig. S4 *A* and *B*. During electrical recordings in dark-adapted conditions, we did not

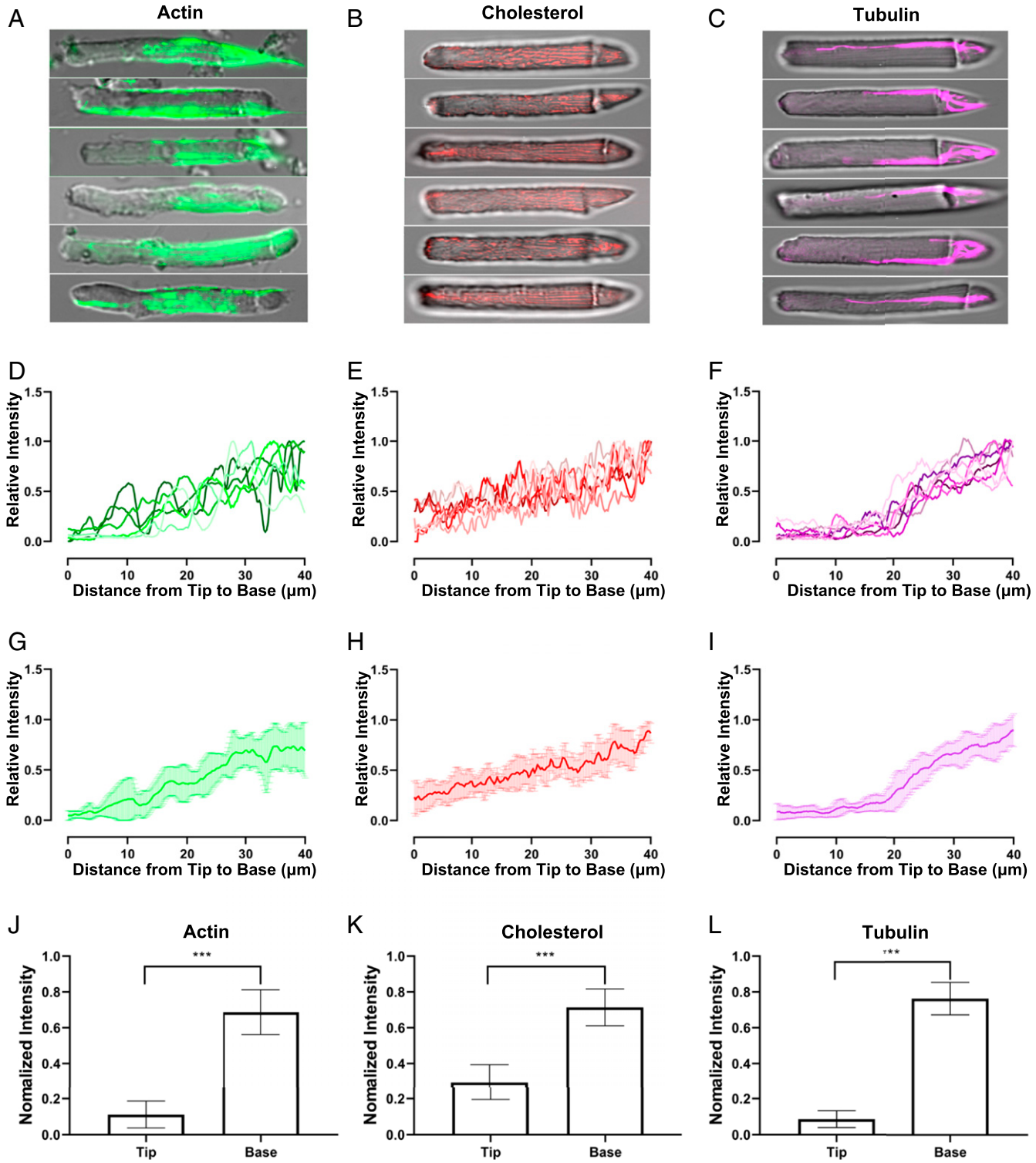

Fig. 6. Actin, tubulin, and cholesterol gradients in rods OSs. (*A*) IS+OS rods, stained with phalloidin. (*B*) As in *A*, but rods were stained with Bodipy marker. (*C*) As in *A*, but rods were stained with tubulin marker. (*D*) Normalized intensity profile obtained from the six representative IS+OS rods in *A*, from the OS base to the tip. (*E*) Same as in *D* but for the cholesterol staining in *B*. (*F*) Same as in *D* but for the tubulin staining in *C*. (*G*) Averaged intensity profile obtained from the six representative IS+OS rods in *A*. (*H*) Same as in *G* but for the cholesterol staining in *B*. (*I*) Same as in *G* but for the tubulin staining in *C*. (*J*) Quantification of the actin staining intensity profile. Base and tip average intensity were 0.687 ± 0.051 SEM and 0.112 ± 0.030 SEM, respectively ($n = 8$; *t* test $P < 0.001$). (*K*) As in *J* but for the cholesterol staining. Base and tip average intensity were 0.714 ± 0.039 SEM and 0.295 ± 0.037 SEM, respectively ($n = 9$; *t* test $P < 0.001$). (*L*) As in *J* but for the tubulin staining. Base and tip average intensity were 0.762 ± 0.034 SEM and 0.086 ± 0.018 SEM, respectively ($n = 7$; *t* test ***$P < 0.001$).

observe any event that could be attributed to the spontaneous calcium flares described in Fig. 4. We are not able to establish whether calcium flares occur in the complete absence of any light stimulation, because they are detected with a fluorescent dye—i.e., CasIR—requiring an excitation light in the near-infrared perceived by the rods.

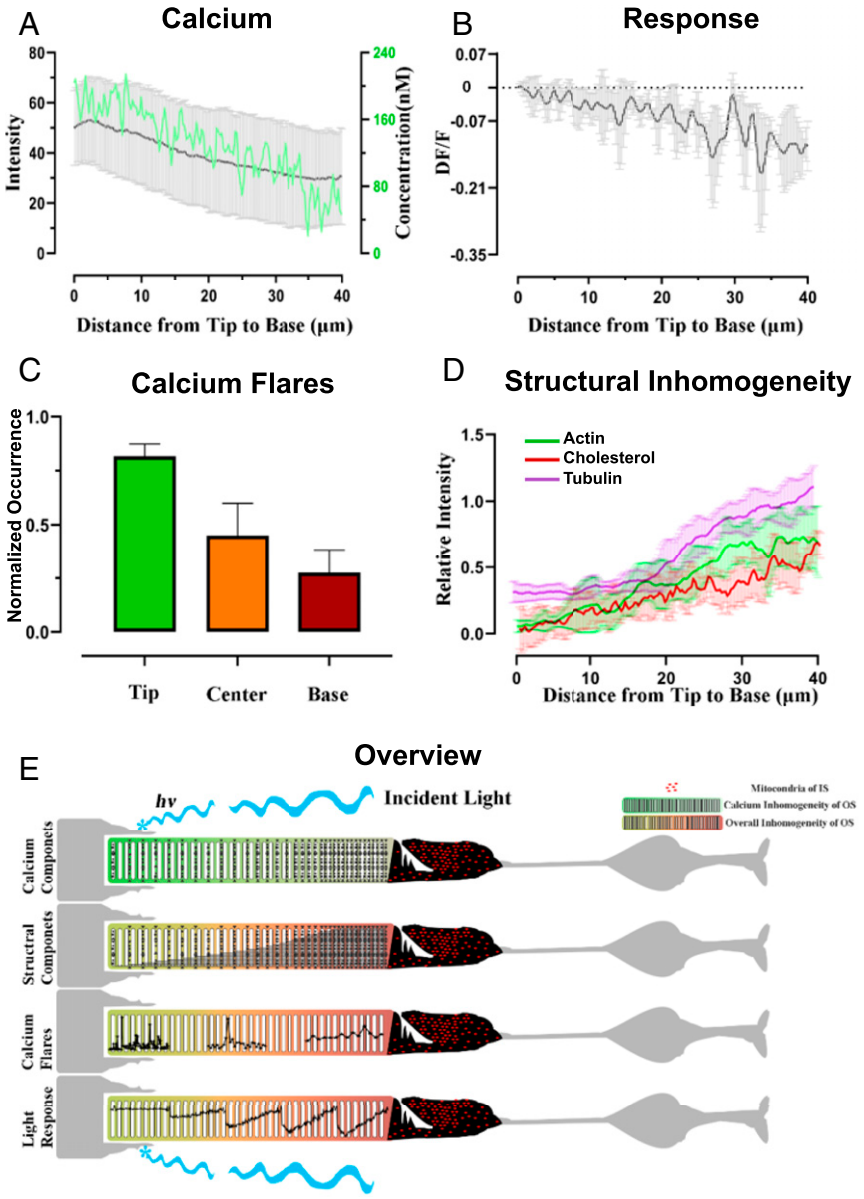

Fig. 7. Structural and functional gradients in OS. (*A*) The gradient of $[Ca^{2+}]_i$ obtained in light-adapted conditions using Fura Red (right axis and see *SI Appendix*, Fig. S3) and of the emitted CaSiR-1 fluorescence in semidark-adapted conditions (left axis) ($n = 8$). (*B*) The gradient of responsiveness ($n = 10$). (*C*) The distribution of calcium flares ($n = 60$; $mean_{base}$ 0.275 ± 0.063 SEM, $mean_{center}$ 0.450 ± 0.087 SEM, $mean_{tip}$ 0.817 ± 0.033 SEM). (*D*) The gradient of actin, tubulin, and cholesterol (see also Fig. 6). (*E*) Summary of the functional and structural gradients presents in the rod OS.

Calcium flares at the OS tip can be triggered by a flash of light at 488 nm, and in these circumstances the same flash of light induces a drop of $[Ca^{2+}]_i$ at the OS base (Fig. 4 *E* and *F*).

Our imaging experiments show that these calcium flares always appear tangentially to the OS and do occur in a restricted longitudinal portion of the OS (Fig. 4*F*). These results suggest that calcium flares colocalize with discs inside the OS, indicating that they probably originate from the discs. We rarely observed light-induced calcium flares at the OS base, which usually appeared only at the center and tip of the OS. We propose, therefore, that calcium flares are part of the disk renewal and shedding process and could signal retinal pigmented epithelium cells to trigger phagocytosis of aged and shedding discs (19, 32, 33).

Longitudinal Inhomogeneity of Rod Outer Segments and Disk Turnover. There are several previous reports indicating heterogeneity in rod OSs, reviewed by Koch and Dell'Orco (34), which has been ascribed to natural aging and renewal of OSs. Several observations indicate that the proteins involved in transduction and adaptation are assembled in complexes forming highly ordered structures that interact with the supporting disk membranes and the local cellular architecture (24, 32). Key proteins involved in phototransduction, such as rhodopsin, transducing, and phosphodiesterase, operate over the discs and are very close to the plasma membrane, where cyclic nucleotide gated channels are located. Indeed, the efficiency of the phototransduction machinery depends on the structural properties of the discs (34, 35), which are affected by the renewal and shedding processes occurring at the base and tip of OSs, respectively. Moreover, the gradient of concentration/abundancy of structural proteins along the OS (Fig. 7*D*) is likely to be the consequence of the renewal and shedding process. In this view, the presence of a functional and structural gradient along the length of

the OS (Fig. 7) is not surprising, in agreement with previous investigations based on the use of Lucifer Yellow (36) and the dye FM1-43 (20).

Calcium Compartmentalization. Previous reports (14, 37) using Ca^{2+} Green and Fura 2 in isolated OSs and in isolated IS+OSs have not detected a calcium gradient in the OS, as observed here (Fig. 1 and *SI Appendix*, Fig. S3). This discrepancy is likely caused by the use of CaSiR-1, which works in the near IR and allows us to verify whether isolated IS+OS are functional. Indeed, we were able to observe a photoresponse, i.e., a light-induced drop in intracellular calcium. We did not observe a calcium gradient in nonfunctional IS+OSs (Fig. 1). The sharp brightness difference in fluorescence observed in functional rods (Fig. 2) between the IS and the base of the OS suggests that there is no or limited fusion of the inner and outer segment membranes (38). Our ratiometric analysis of calcium concentration in the IS+OS indicates that the levels of calcium measured in the IS are 65 ± 2.63 nM, a value in the range of what was previously reported (39). Therefore, the strong fluorescence observed in IS+OS loaded with CaSiR-1 AM possibly reflects a calcium concentration at the physiological level.

A remarkable feature of calcium dynamics in rods is the relative isolation of the OS and IS (Fig. 5). Calcium changes that have initiated either in the IS or in the OS do not easily propagate through the cilium connecting the OS and the IS, which is known to provide electrical coupling (27). The strong compartmentalization of calcium dynamics between the IS and OS is likely to be caused by the high density of mitochondria present in the IS near the cilium (Fig. 5*D*), which act as a powerful buffer of $[Ca^{2+}]_i$ and, thus, as a barrier for the diffusion of intracellular calcium between the OS and IS. Calcium flares originating in the OS do not diffuse easily along the OS, as could be expected in the restricted free space inside the OSs. Indeed, the presence of the inner segment affects the localization of proteins already present in the outer segment. In support of this view (Fig. 2), intact rods from a piece of retina have a much reduced and often almost absent photoresponse at the tip. This observation indicates that proteins present in the IS and nucleus affect properties of the phototransduction cascade in the OS. Interestingly, based on a recent study conducted in zebrafish (40), it was reported that variations in calcium in the mitochondria of cone photoreceptors can influence both phototransduction and the metabolism of these neurons. Moreover, it has been shown that mitochondria strictly regulate calcium concentration inside rod photoreceptors and that an imbalance in their membrane potential leads to apoptosis (41). We have not observed calcium flares in isolated OS, and we believe that the renewal process of discs observed in intact and functional rods occurs because discs deteriorate and flares—in our view—are linked to their renewal.

In the rod OS, there is a powerful mechanism for the extrusion of Ca^{2+} consisting of Na^+: Ca^{2+}, K^+ (NCKX1), which has been characterized in great detail (15). It has been shown that rods in which the gene encoding NCKX1 has been knocked out are functional to some extent (42). This observation suggests the existence of additional molecular mechanisms able to extrude calcium from the interior of the OS. A high density of these molecular mechanisms in the OS can be a barrier impeding the longitudinal diffusion of intracellular calcium. The extrusion of Ca^{2+} from the rod OS is mediated by the Na^+: Ca^{2+}, K^+ exchanger (43). In darkness, the extrusion of one Ca^{2+} and one K^+ requires the entry of four Na^+ ions (44). Na^+ ions entering the OS through the light-sensitive channels are extruded by the Na^+/K^+-ATPase located in the IS (15); therefore, the concentration of intracellular Na^+ is higher at the tip than at the base, where there is a sink for Na^+. There are no known Na^+ buffers, and the Na^+ diffusion coefficient is ∼1,900 $\mu m^2 \cdot sec^{-1}$, which is much larger than that of cGMP. We expect Na^+ to diffuse freely within most of the OS, and we do not expect a large Na^+ gradient for most of the OS length. However, given the steep dependence of the activity of the Na^+: Ca^{2+}, K^+ exchanger on the Na^+ concentration, even a shallow Na^+ gradient within the OS could be responsible for the calcium gradient we observed within the OS. This shallow Na^+ gradient is expected to have only a small effect on the amplitude of the photoresponse, which depends linearly on the Na^+ gradient.

Given the functional and structural gradient of the phototransduction machinery (Fig. 7), in order to maximize the detection of photons, it is convenient that photons arriving from the external world impinge first on the OS base. Indeed, this could be one of the reasons for the geometrical arrangement of the retina inside the eye in which photons travel through the entire retina before reaching the rods: In this way, the first encountered rhodopsin molecules are those located at the OS base that efficiently initiate phototransduction.

Methods

Immunofluorescence. Single-rod staining was obtained by fixing the retina in paraformaldehyde solution at 4% for 60 min at 22–25 °C. The tissue was then permeabilized with a solution of phosphate-buffered saline (PBS) with 0.1% Triton X-100. A PBS solution with bovine serum albumin at 1% was used to block not-specific binding sites. Then, the retina was washed with cold PBS three times for 5 min each. The incubation of the retina with Phalloidin (Life Technologies, A12379, Ringer solution 1:4,000) at room temperature for 1 h allowed the visualization of the actin in the tissue. Single rods were then obtained by mechanical dissociation and examined with a confocal microscope (NIKON A1R) equipped with 488-nm and 640-nm excitation lasers, 40× objective (N.A. 0.75) and 60× oil immersion objective (N.A. 1.40).

Isolation of Photoreceptors and Electrical Recordings. The experiments described in this paper followed the guidelines of the International School for Advanced Studies ethics committee and the Italian and European procedures for animal care (d.l. 116/92; 86/609/C.E.). Male and female frogs of the species *X. laevis* were dark adapted overnight, anesthetized with tricaine, and euthanized under dim red light. Their eyes were dissected as previously reported (45). Single rods consisting of an IS+OS were obtained by gentle mechanical dissociation of a small piece of retina, cut from the whole with surgical scissors. The integrity of the isolated retinal rods was maintained immersing them in Ringer solution containing (in mM): 110 NaCl, 2.5 KCl, 1 $CaCl_2$, 1.6 $MgCl_2$, and 3 Hepes-NaOH, 0.01 EDTA, and 10 glucose (pH 7.7–7.8 buffered with NaOH). The experiments were performed at 22–25 °C, and the salts and chemicals were purchased from Sigma-Aldrich.

The recording of rod photoreceptors light response (*SI Appendix*, Fig. S2) were obtained as previously described (45). The Axopatch 200A (Molecular Devices, LLC) was used in voltage clamp mode to record the sensory neurons currents, which were digitized at 10 kHz and low-pass filtered at 20 Hz. The filtering and the correction of the baseline was done with Clampfit 10.3 (Molecular Devices). To activate phototransduction, brief (10-ms) blue laser light pulses at 491-nm wavelength (Rapp OptoElectronic) emerged from a 10× objective of an inverted microscope (Olympus IX71; Olympus Corporation). The resulting circular spot of ∼60 μm in diameter was used to stimulate uniformly the rods. Two cameras (Hamamatsu ORCA-Flash 4.0, Hamamatsu Corporation; and Jenoptic ProgRes MF, JENOPTIK I Optical Systems, Goeschwitzer) were used to visualized the cells to avoid changing the objectives (11).

Calcium Imaging and Other Fluorescence Imaging. Retinas were immersed in the Ringer solution described in the previous section and loaded with a final concentration of 5 μM of the cell-permeable calcium dye CaSiR-1 AM (previously Goryo chemicals; currently it is the BioTracker 664 NIR Ca^{2+} Dye, Millipore Sigma) at room temperature (22–25 °C) for 45 min. After incubation, the retinas were washed three times, for 5 min each time, allowing the intracellular deesterification of the dye. Small pieces of retinas were mechanically dissociated as described above and the isolated rods were transferred into a light sealed chamber. The chamber was then placed on the stage of an Olympus IX-81 inverted microscope equipped with a light-emitting diode (LED) illumination system (X-Cite XLED1 from Excelitas Technologies), which was used for both calcium imaging (650-nm light) and light stimulations (488 nm). The experiments were performed at room temperature (between 22 and 25 °C), and the images were acquired using Micromanager software with an Apo-Fluor 60×/1.4 N.A. objective, at a sampling rate of 5 Hz for 3–10 min.

Mitotracker imaging (Life Technologies, M7512) was performed on very fresh retinas, which were immersed in Ringer solution and loaded with a final concentration of the dye of 100 nM, at 22–25 °C for 45 min in darkness. Then, they were mechanically dissociated, and the fluorescence was imaged using

560-nm LED excitation, on an Olympus IX-81 inverted microscope system. For tubulin tracker imaging (Life Technologies, T34077), we used the same incubation protocol as for the mitotracker imaging, but the final concentration of the dye was 200 nM and the incubation period lasted 1 h at 22–25 °C. The fluorescent imaging was done with a confocal microscope (NIKON A1R) and a laser at 640-nm excitation light. The objective used to visualize the cells were the 40× objective (N.A. 0.75) and 60× oil immersion objective (N.A. 1.40) mentioned previously. Cholesterol imaging was performed using the Bodipy dye (Life Technologies, C12680). Retinas were loaded as described above, but with a final dye concentration of 100 nM, and incubated in darkness for over 3 h or overnight at 4 °C. The imaging was performed with the same Nikon confocal microscope, but with an excitation laser at 514-nm wavelength. For Fura Red (Life Technologies, F3020) ratiometric calcium imaging, the dye was used at a final concentration of 5 μM in Ringer solution, and retinas were incubated for 1 h in darkness at 22–25 °C. The 488-nm LED excitation was chosen for general fluorescent imaging, and 440 nm/480 nm was used for the ratiometric experiments. For the localized light stimulations, the Nikon confocal microscope was set under the acquisition controls of A1plus stimulation. Excitation laser was set at low intensity as the stimulation light. Under non-diffused 488-nm light stimulation, the regions of interest were drawn as needed on the desired rods for local stimulations of light and then added into the serial acquisition phases. The frame time was set as less than 150 ms.

Mechanical Stimulation Using the Oscillatory Optical Trap. The mechanical stimulation of the photoreceptors was performed as previously described (46). Briefly, a polystyrene bead of 3.5 μm in diameter (G. Kisker GbR) was manipulated with an oscillatory optical trap, obtained using a Focused Tunable Lens (FTL) (EL-10-30-NIR-LD, Optotune AG). The bead was moved above the rods and sealed to the membrane. Rods stimulation was achieved precisely by tuning the FTL to change the vertical position of a bead trapped with the infrared laser. A sinusoidal pulse was sent from the computer to the FTL controller, which resulted in the oscillation of the lens and the change of the focal plane of the trapped bead. This technique allowed a confined indentation of the rods' membrane. A complete description of the method and of all of the components used can be found in the citations (46).

Data and Statistical Analysis. The *DF/F* of calcium imaging experiments was quantified using a custom Matlab code (MathWorks, Inc.) and ImageJ software v1.6 (NIH). All of the results here described are presented as mean ± SEM. The Student's *t* test (GraphPad Prism 7, GraphPad software) was used to quantify the statistical significance of the results.

Data Availability. All study data are included in the article and supporting information. All of the data used to plot panels are available in Dataset S1.

ACKNOWLEDGMENTS. We thank Daniele Dell Orco, Hugh Robinson, and Vadim Arshavsky for their useful and critical reading of the manuscript. This work was supported by funds from Regione Friuli-Venezia Giulia (Italy) for the project "GLIOBLASTOMA–Infiltrazione nei gliomi: nuovo target terapeutico"; 3315 Innovative Teams Program of Ningbo–China, Zhejiang Provincial Natural Science Foundation of China Grant LQ17C100001; and Natural Science Foundation of Ningbo City Grant 2017A610256.

1. P. A. Liebman, H. L. Weiner, R. E. Drzymala, Lateral diffusion of visual pigment in rod disk membranes. *Methods Enzymol.* **81**, 660–668 (1982).
2. I. Nir, M. O. Hall, The ultrastructure of lipid-depleted rod photoreceptor membranes. *J. Cell Biol.* **63**, 587–598 (1974).
3. J. C. Gilliam *et al*., Three-dimensional architecture of the rod sensory cilium and its disruption in retinal neurodegeneration. *Cell* **151**, 1029–1041 (2012).
4. W. J. Spencer *et al*., Photoreceptor disc membranes are formed through an Arp2/3-dependent lamellipodium-like mechanism. *Proc. Natl. Acad. Sci. U.S.A.* **116**, 27043–27052 (2019).
5. O. P. Kocaoglu *et al*., Photoreceptor disc shedding in the living human eye. *Biomed. Opt. Express* **7**, 4554–4568 (2016).
6. K. Boesze-Battaglia, T. Hennessey, A. D. Albert, Cholesterol heterogeneity in bovine rod outer segment disk membranes. *J. Biol. Chem.* **264**, 8151–8155 (1989).
7. K. Boesze-Battaglia, A. D. Albert, Cholesterol modulation of photoreceptor function in bovine retinal rod outer segments. *J. Biol. Chem.* **265**, 20727–20730 (1990).
8. K. Boesze-Battaglia, S. J. Fliesler, A. D. Albert, Relationship of cholesterol content to spatial distribution and age of disc membranes in retinal rod outer segments. *J. Biol. Chem.* **265**, 18867–18870 (1990).
9. J. L. Schnapf, Dependence of the single photon response on longitudinal position of absorption in toad rod outer segments. *J. Physiol.* **343**, 147–159 (1983).
10. T. D. Lamb, P. A. McNaughton, K.-W. Yau, Spatial spread of activation and background desensitization in toad rod outer segments. *J. Physiol.* **319**, 463–496 (1981).
11. M. Mazzolini *et al*., The phototransduction machinery in the rod outer segment has a strong efficacy gradient. *Proc. Natl. Acad. Sci. U.S.A.* **112**, E2715–E2724 (2015).
12. D. A. Baylor, T. D. Lamb, Local effects of bleaching in retinal rods of the toad. *J. Physiol.* **328**, 49–71 (1982).
13. K. J. Miyagishima, M. C. Cornwall, A. P. Sampath, Metabolic constraints on the recovery of sensitivity after visual pigment bleaching in retinal rods. *J. Gen. Physiol.* **134**, 165–175 (2009).
14. M. Gray-Keller, W. Denk, B. Shraiman, P. B. Detwiler, Longitudinal spread of second messenger signals in isolated rod outer segments of lizards. *J. Physiol.* **519**, 679–692 (1999).
15. L. Lagnado, L. Cervetto, P. A. McNaughton, Calcium homeostasis in the outer segments of retinal rods from the tiger salamander. *J. Physiol.* **455**, 111–142 (1992).
16. S. Forti, A. Menini, G. Rispoli, V. Torre, Kinetics of phototransduction in retinal rods of the newt Triturus cristatus. *J. Physiol.* **419**, 265–295 (1989).
17. A. P. Sampath, H. R. Matthews, M. C. Cornwall, G. L. Fain, Bleached pigment produces a maintained decrease in outer segment Ca2+ in salamander rods. *J. Gen. Physiol.* **111**, 53–64 (1998).
18. A. Majumder *et al*., Exchange of cone for rod phosphodiesterase 6 catalytic subunits in rod photoreceptors mimics in part features of light adaptation. *J. Neurosci.* **35**, 9225–9235 (2015).
19. G. L. Fain, W. H. Schröder, Light-induced calcium release and re-uptake in toad rods. *J. Neurosci.* **10**, 2238–2249 (1990).
20. C. Chen, Y. Jiang, Y. Koutalos, Dynamic behavior of rod photoreceptor disks. *Biophys. J.* **83**, 1403–1412 (2002).
21. T. Egawa *et al*., Development of a far-red to near-infrared fluorescence probe for calcium ion and its application to multicolor neuronal imaging. *J. Am. Chem. Soc.* **133**, 14157–14159 (2011).
22. M. Oheim *et al*., New red-fluorescent calcium indicators for optogenetics, photoactivation and multi-color imaging. *Biochim. Biophys. Acta* **1843**, 2284–2306 (2014).
23. U. Bocchero *et al*., Mechanosensitivity is an essential component of phototransduction in vertebrate rods. *PLoS Biol.* **18**, e3000750 (2020).
24. G. M. Ratto, R. Payne, W. G. Owen, R. Y. Tsien, The concentration of cytosolic free calcium in vertebrate rod outer segments measured with fura-2. *J. Neurosci.* **8**, 3240–3246 (1988).
25. T. D. Lamb, E. N. Pugh, Phototransduction in vertebrate rods and cones: Molecular mechanisms of amplification, recovery and light adaptation. *Handb. Biol. Phys.* **3**, 183–255 (2000).
26. T. Burgoyne *et al*., Rod disc renewal occurs by evagination of the ciliary plasma membrane that makes cadherin-based contacts with the inner segment. *Proc. Natl. Acad. Sci. U.S.A.* **112**, 15922–15927 (2015).
27. H. Khanna, Photoreceptor sensory cilium: Traversing the ciliary gate. *Cells* **4**, 674–686 (2015).
28. M. M. Giarmarco, W. M. Cleghorn, S. R. Sloat, J. B. Hurley, S. E. Brockerhoff, Mitochondria maintain distinct Ca2+ pools in cone photoreceptors. *J. Neurosci.* **37**, 2061–2072 (2017).
29. F. S. Sjöstrand, The ultrastructure of the outer segments of rods and cones of the eye as revealed by the electron microscope. *J. Cell. Comp. Physiol.* **42**, 15–44 (1953).
30. S. Nickell, P. S. H. Park, W. Baumeister, K. Palczewski, Three-dimensional architecture of murine rod outer segments determined by cryoelectron tomography. *J. Cell Biol.* **177**, 917–925 (2007).
31. M. M. LaVail, Rod outer segment disk shedding in rat retina: Relationship to cyclic lighting. *Science* **194**, 1071–1074 (1976).
32. P. Nunes, N. Demaurex, The role of calcium signaling in phagocytosis. *J. Leukoc. Biol.* **88**, 57–68 (2010).
33. S. Zumerle *et al*., Intercellular calcium signaling induced by ATP potentiates macrophage phagocytosis. *Cell Rep.* **27**, 1–10.e4 (2019).
34. K.-W. Koch, D. Dell'Orco, Protein and signaling networks in vertebrate photoreceptor cells. *Front. Mol. Neurosci.* **8**, 67 (2015).
35. T. G. Wensel, Signal transducing membrane complexes of photoreceptor outer segments. *Vision Res.* **48**, 2052–2061 (2008).
36. B. Matsumoto, J. C. Besharse, Light and temperature modulated staining of the rod outer segment distal tips with Lucifer yellow. *Invest. Ophthalmol. Vis. Sci.* **26**, 628–635 (1985).
37. D. Krizaj, D. R. Copenhagen, Compartmentalization of calcium extrusion mechanisms in the outer and inner segments of photoreceptors. *Neuron* **21**, 249–256 (1998).
38. E. Townes-Anderson, Intersegmental fusion in vertebrate rod photoreceptors. Rod cell structure revisited. *Invest. Ophthalmol. Vis. Sci.* **36**, 1918–1933 (1995).
39. T. Szikra, D. Krizaj, The dynamic range and domain-specific signals of intracellular calcium in photoreceptors. *Neuroscience* **141**, 143–155 (2006).
40. R. A. Hutto *et al*., Increasing Ca^{2+} in photoreceptor mitochondria alters metabolites, accelerates photoresponse recovery, and reveals adaptations to mitochondrial stress. *Cell Death Differ.* **27**, 1067–1085 (2020).
41. L. He, A. T. Poblenz, C. J. Medrano, D. A. Fox, Lead and calcium produce rod photoreceptor cell apoptosis by opening the mitochondrial permeability transition pore. *J. Biol. Chem.* **275**, 12175–12184 (2000).
42. F. Vinberg, J. Chen, V. J. Kefalov, Regulation of calcium homeostasis in the outer segments of rod and cone photoreceptors. *Prog. Retin. Eye Res.* **67**, 87–101 (2018).
43. L. Cervetto, L. Lagnado, R. J. Perry, D. W. Robinson, P. A. McNaughton, Extrusion of calcium from rod outer segments is driven by both sodium and potassium gradients. *Nature* **337**, 740–743 (1989).
44. L. Lagnado, L. Cervetto, P. A. McNaughton, Ion transport by the Na-Ca exchange in isolated rod outer segments. *Proc. Natl. Acad. Sci. U.S.A.* **85**, 4548–4552 (1988).
45. U. Bocchero, B. M. Tam, C. N. Chiu, V. Torre, O. L. Moritz, Electrophysiological changes during early steps of retinitis pigmentosa. *Invest. Ophthalmol. Vis. Sci.* **60**, 933–943 (2019).
46. F. Falleroni, V. Torre, D. Cojoc, Cell mechanotransduction with piconewton forces applied by optical tweezers. *Front. Cell. Neurosci.* **12**, 1–11 (2018).